



CrossMark

Dating and Tracing the Origin of Enstatite Chondrite Chondrules with Cr Isotopes

Ke Zhu (朱柯)¹ , Frédéric Moynier¹, Martin Schiller² , and Martin Bizzarro^{1,2} ¹ Institut de Physique du Globe de Paris, Université de Paris, CNRS UMR 7154, 1 rue Jussieu, Paris F-75005, France; zhu@ipggp.fr² Centre for Star and Planet Formation, Globe Institute, University of Copenhagen, Øster Voldgade 5–7, Copenhagen DK-1350, Denmark

Received 2020 March 29; revised 2020 April 27; accepted 2020 April 28; published 2020 May 14

Abstract

Chondrules are major components of chondrites and are believed to drive the accretion of planetary embryos. As such, constraining the timing and origin of chondrules is central for understanding the early evolution of the solar system and the formation of planets. Enstatite chondrites (ECs) have isotope compositions for multiple elements that match that of the Earth and, thus, are considered to be good analogs of the precursor material from which the Earth formed. Here, we report the first high-precision mass-independent Cr isotope data of nine chondrules in one of the least-altered EH chondrites, Sahara 97096. Seven primitive chondrules show typical $^{54}\text{Cr}/^{52}\text{Cr}$ ratios of bulk ECs, whereas two chondrules have ratios similar to carbonaceous chondrites. The presence of two chondrules with a carbonaceous chondrite signature suggests early inward transport of material to the EC accretion region. The Mn/Cr ratios of the EC-like chondrules (except one with high Fe content) correlate with their $^{53}\text{Cr}/^{52}\text{Cr}$ isotope ratios, which we interpret as a fossil isochron, with a slope corresponding to a $^{53}\text{Mn}/^{55}\text{Mn}$ initial ratio of $(5.01 \pm 0.59) \times 10^{-6}$ (2σ). When anchored to the D'Orbigny angrite, this $^{53}\text{Mn}/^{55}\text{Mn}$ ratio returns an absolute age of 4565.7 ± 0.7 Ma for EC chondrule formation (precursor age), 1.6 ± 0.7 Ma after solar system formation. This protracted formation of EC chondrules may suggest that the mass transfer of outer solar system material started prior to the end of planetary embryo accretion, as chondrules could represent the main building blocks of terrestrial planets.

Unified Astronomy Thesaurus concepts: Astrochemistry (75); Cosmochemistry (331); Cosmochronology (332); Solar system (1528); Isotopic abundances (867); Meteoroids (1040); Chondrules (229); Nucleosynthesis (1131); Chondrites (228)

1. Introduction

Chondrules, millimeter-sized silicate spheres with igneous textures, are the major components of most chondrites (Hewins 1997) and potentially represent the building blocks of planetary embryos (Johansen et al. 2015). Although deciphering chondrule formation is critical to understanding the growth of terrestrial planets, the precise mechanisms and timing of chondrule formation is still unclear. Among the chondrules from different chondrites, enstatite chondrite (EC) chondrules are dominated by Fe-poor enstatites ($\sim 70\%$), and also contain some olivine, mesostasis, and sulfide opaque minerals (Lehner et al. 2013; Piani et al. 2016; Jacquet et al. 2018). More importantly, ECs best match the Earth in terms of isotopic compositions (Javoy et al. 2010; Moynier & Fegley 2015). Therefore, the chondrules of ECs may be promising candidates as precursor analogs of the solids that accreted to form the Earth and, perhaps the Moon given their close isotopic match (e.g., Zhang et al. 2012; Connelly & Bizzarro 2016; Mougél et al. 2018). Furthermore, given the possibly similar chemical composition (e.g., Fe/Si ratio) and reduced state of Mercury, ECs may also have a close connection to this planet (Wasson 1988; Ebel & Alexander 2011; Nittler & Weider 2019).

Despite the possible importance of EC chondrules with regard to Earth's accretion, their formative age is still unknown, which is mostly due to the challenging nature of obtaining precise age information from these materials. These challenges include the overabundance of common Pb, essentially reflecting the fact that the U/Pb ratios of the chondrules are close to the solar value. As such, it is not possible to obtain useful age information (J. Connelly 2020, personal communication). Moreover, The scarcity of Al-rich minerals (with high Al/Mg, e.g., plagioclase)

in EC chondrules (Piani et al. 2016) limits the possibility of obtaining high-precision ^{26}Al - ^{26}Mg isochron. As for the rare Al-rich chondrules in ECs, furthermore, Guan et al. (2006) found that there is much less resolvable excess ^{26}Mg from the in situ decay of ^{26}Al in these chondrules, and also failed to date the EC Al-rich chondrules by Al-Mg chronometry. As for another well and frequently used chronometry, the ^{182}Hf - ^{182}W system, W is not abundant enough so that its isotopic composition can be measured in individual chondrules. Hf-W isochrons have been reported for pooled chondrule and matrix aliquots (e.g., Budde et al. 2016b, 2018). However, the distinct nucleosynthetic composition of the chondrule and matrix (Budde et al. 2016a) indicated that these objects are not genetically related, which violates the primary assumption of an isochron. As such, the Hf-W correlation lines most likely represent mixing lines that have no chronological information (Connelly & Bizzarro 2018; Zhu et al. 2019a). As such, no solid age constraints exist for EC chondrules.

To unravel the formation age of EC chondrules, the ^{53}Mn -to- ^{53}Cr decay system is the most suitable (Birck & Allègre 1988; Lugmair & Shukolyukov 1998; Trinquier et al. 2008b; Zhu et al. 2019a, 2019b, 2020c), because (1) ^{53}Mn has a half-life of 3.7 Ma and, therefore, its decay to ^{53}Cr can be used for chronometry during the first 10 Ma of the solar system; (2) Cr is relatively abundant in chondrules (>3000 ppm; e.g., Alexander et al. 2008), which therefore allows precise measurement of its isotopic composition, even in sub-mg samples; (3) the variation of the Mn/Cr ratios between EC chondrules (with values from 0.1 to more than 1) is large enough to ensure high-precision ages (Schneider et al. 2002); (4) the good concordance between U-Pb and ^{53}Mn - ^{53}Cr ages of Gujba CB chondrules (Bollard et al. 2015), bulk angrites (Zhu et al. 2019b), and one carbonaceous achondrite (Amelin et al. 2019; Sanborn et al. 2019) supports an

initially homogeneous distribution of the $^{53}\text{Mn}/^{55}\text{Mn}$ ratio throughout the solar system.

It should be noted that different isochrons dating chondrules reflect different stages of chondrule formation. The Pb–Pb and in situ internal Al–Mg chondrule ages reflect the lasting melting ages (e.g., Connelly & Bizzarro 2018; Nagashima et al. 2018), while the external isochrons (e.g., Mn–Cr and Al–Mg) established by multiple chondrules date the formation of chondrule precursors (instead of the average lasting melting ages; e.g., Yin et al. 2009; Yamashita et al. 2010; Luu et al. 2015; Zhu et al. 2019a). Theoretically, the last-melting ages cannot predate the precursor ages. This is similar to the angrite chronology that the bulk Mn–Cr isochron age (reflecting the differentiation of angrite parent body) for all the angrites is older than or similar to Pb–Pb, Mn–Cr and Hf–W internal isochron ages (reflecting the crystallization ages for single angrites; see Figure 3 in Zhu et al. 2019b).

The variation in the $^{54}\text{Cr}/^{52}\text{Cr}$ ratios among meteorites results from the heterogeneous distribution of carriers with nucleosynthetic anomalies between meteorite groups, which could be an effective tracer to study the genetic relationships of chondrules (Trinquier et al. 2007). Some carbonaceous chondrites' (CC) and ordinary chondrites' (OC) chondrules exhibit $^{54}\text{Cr}/^{52}\text{Cr}$ ratio heterogeneities (Qin et al. 2011; Connelly et al. 2012; Olsen et al. 2016; van Kooten et al. 2016; Bollard et al. 2019; Zhu et al. 2019a), which suggests that the chondrule precursors might be mixed and did not only originate from their host chondrite. It also indicates that bulk chondrite compositions of these chondrite groups were modified by radial transport of solar system materials. However, it is not known whether EC chondrules exhibit similar variability in $^{54}\text{Cr}/^{52}\text{Cr}$ ratios. Furthermore, investigating the Cr isotope composition of EC chondrules can be used to test the possible chondrule-matrix complementarity within ECs (e.g., Hezel et al. 2018).

Here, we report the first mass-independent Cr isotopic data for individual EC chondrules. Variations in the $^{54}\text{Cr}/^{52}\text{Cr}$ ratios for individual EC chondrules are used to discuss their origin and the implications for the evolution of early solar system materials. Furthermore, we define a ^{53}Mn – ^{53}Cr bulk isochron, which we interpret to represent the first accurate age for EC chondrules formation.

2. Samples and Analytical Methods

For this study, we selected one of the most primitive EC of type EH3, Sahara 97096, which experienced no aqueous alteration and limited thermal metamorphism (Weisberg & Kimura 2012). Based on the organization degree of its organic matter, Sahara 97096 has been classified as the type of EH3.1 ~ 3.4 (Quirico et al. 2011). Furthermore, the cosmic-ray exposure age (less than 20 Ma Patzer & Schultz 2001) and low Fe/Cr ratio (dominated by Fe-poor enstatites) for Sahara 97096 imply that the primitive Cr isotope compositions was not detectably altered by cosmic-ray irradiation.

Polished sections of the Sahara 97096 were imaged and studied using a Zeiss EVO MA10 scanning electron microscope (SEM) located at the Institute de Physique du Globe de Paris (IPGP), France. Our objectives during the initial characterization were to select chondrules of diverse sizes, chemical compositions (S, Si, Fe, Mn, Cr, Mg, Ca, Ti, Ni, Na distribution were detected by X-ray mapping) and petrological textures (see Figures A1 and A2 in Appendix). Fourteen selected chondrules were carefully extracted using a New

Wave microdrill with tungsten carbide drill bits at IPGP and thereafter transferred to clean Teflon Bombs for further dissolution following methods detailed in van Kooten et al. (2017). The chondrule sizes ranged between 0.3 and 1 mm and were not excavated too deep (~100 μm) to avoid contamination of the drill sample with surrounding material. All drill spots were carefully examined under a plain-light microscope and drill spots where contamination was suspected were discarded. We drilled approximately several cylindrical holes (20 μm diameter, 100 μm depth) per sample, yielding more than 200 ng of Cr.

The samples were first dissolved in sealed in Teflon Bombs in a mixture of concentrated HF and HNO_3 (2:1) that were heated in an Analab EvapoClean at 140°C for two days following method detailed in Inglis et al. 2018 and Zhu et al. 2019b. Subsequently, samples were further dissolved in aqua regia (concentrated HCl and HNO_3 mixture in 3:1 ratio, also at 140°C) for another two days to ensure complete digestion of fluorides and refractory phases such as chromite and spinel. After dissolution, 10% of aliquots were extracted for elemental analysis using inductively coupled plasma mass spectrometry (ICP-MS) for major element content and multiple collector inductively coupled plasma mass spectrometry (MC-ICP-MS) using a Thermo-Fisher Scientific Neptune Plus for $^{55}\text{Mn}/^{52}\text{Cr}$ ratio measurements at IPGP, following the method described in Göpel et al. (2015). The estimated external precision of these approaches are 5% ~ 10% for major element concentrations and <5% for the $^{55}\text{Mn}/^{52}\text{Cr}$ ratios (Zhu et al. 2020c). Based on the elemental content information, we finally selected nine chondrule samples with varied Mn/Cr and Cr content more than 200 ng for the following Cr isotope studies.

Chromium was purified based on a procedure involving a three-step chromatographic ion-exchange purification protocol, which has been applied in our previous studies (Zhu et al. 2019b). In summary, anion chromatographic purification columns were used to efficiently remove Fe from the remaining sample aliquot in 6M HCl, followed by elution of Cr through a cation exchange column in 0.5M HNO_3 (Bizzarro et al. 2011) and subsequent elution of Mg, Ca, Mn, and Ni in 6M HCl. Prior to sample loading on the cation exchange column, we used a Cr pre-treatment procedure involving dissolution in 10M HCl at >120°C to efficiently promote the formation of Cr(III)–Cl species, which have a low affinity for the cation exchanger and thus elute early (Trinquier et al. 2008a; van Kooten et al. 2016). The third ion-exchange column step aimed at Cr purification from the potential interfering elements Fe (and other high-field-strength elements such as Ti and V) and Na (as well as potential organics) by using a small cation exchange column and 0.5M HNO_3 , 1M HF and 6M HCl as eluants (Larsen et al. 2018). Prior to sample loading onto this last column, Cr was pre-treated by exposure to 0.5M HNO_3 + 0.6% H_2O_2 at room temperature for two days to promote the formation of Cr^{3+} (Larsen et al. 2016). The total yields for this purification range from 88% to 98% and chromium total chemistry blanks are smaller than 2 ng and, thus, negligible compared to the processed more than 200 ng of Cr. After chemistry, the final Cr solution was fluxed for 1 day in 250 ml concentrated aqua regia and concentrated HNO_3 , respectively, to minimize residual organics (i.e., introduced from the cation exchange resin).

The Cr isotopic composition of nine chondrules and bulk sample for Sahara 97096 and Allende chondrite was measured

Table 1
Mn–Cr and Elemental Data for Allende and Sahara 97096 and Chondrules (Named KF) Therein

Sample Name	Cr (ng)	$^{55}\text{Mn}/^{52}\text{Cr}$	$\epsilon^{53}\text{Cr}$	2SE	$\epsilon^{54}\text{Cr}$	2SE	N	Mg#	Al/Mg	Fe/Cr
Sahara 97096		0.65	0.19	0.04	-0.01	0.14	14			
KF1	307	0.35	0.03	0.05	-0.10	0.15	15	95	0.03	8.2
KF2	575	1.56	0.53	0.07	-0.12	0.15	13	97	0.07	7.6
KF4	248	1.89	0.41	0.03	-0.18	0.06	17	88	0.04	18.1
KF5	570	0.04	-0.09	0.05	-0.08	0.12	14	92	0.06	9.7
KF6	434	0.25	-0.16	0.09	-0.04	0.20	11	92	0.05	8.7
KF8	374	0.08	-0.18	0.03	1.01	0.11	14	95	0.05	5.0
KF9	364	0.38	0.01	0.07	0.32	0.11	13	94	0.06	7.8
KF13	804	0.05	-0.08	0.06	-0.03	0.14	22	91	0.05	8.5
KF14	487	0.12	-0.12	0.06	-0.21	0.16	17	97	0.05	4.8
Allende		0.42	0.16	0.06	0.88	0.17	15			
NIST SRM 979			0.00	0.02	0.00	0.04	66			

Note. The masses for these chondrules are less than 0.2 mg, and could not be weighed precisely. N is the number of measurements. The Cr content has an uncertainty (2σ) of 5%–10%. Mg# [(Mg/Mg+Fe)*100%], Al/Mg and Fe/Cr are calculated by atom ratios, with uncertainty (2σ) of 5%.

on the Thermal Ionization Mass Spectrometer (TIMS) Thermo Scientific TRITON at the Centre for Star and Planet Formation, University of Copenhagen. The total-evaporation method was used as described in the previous studies (van Kooten et al. 2016; Zhu et al. 2019b). Around 10–15 ng of Cr was loaded on each filament (tungsten), which can be run \sim 20 minutes. Prior to the Cr isotope measurements, filaments were pre-heated to \sim 800°C for 20 minutes to evaporate residual Na and K left in the sample. Each sample was measured 11–22 times, spanned to two to four turrets, subject to the available Cr amount and present data precision. The $^{53}\text{Cr}/^{52}\text{Cr}$ and $^{54}\text{Cr}/^{52}\text{Cr}$ ratios were normalized to a constant $^{50}\text{Cr}/^{52}\text{Cr}$ ratio of 0.051859 using the exponential law (Lugmair & Shukolyukov 1998). All the measured isotopic ratios are reported relative to NIST SRM 979 that possesses $^{53}\text{Cr}/^{52}\text{Cr}$ and $^{54}\text{Cr}/^{52}\text{Cr}$ of 0.113387 and 0.028222, respectively (Coplen et al. 2002), and expressed in the epsilon notations:

$$\epsilon^x\text{Cr} = \left(\frac{(^x\text{Cr}/^{52}\text{Cr})_{\text{sample}}}{(^x\text{Cr}/^{52}\text{Cr})_{\text{NIST SRM 979}}} - 1 \right) \times 10,000, \quad (1)$$

with $x = 53$ or 54 .

3. Results

The Cr isotopic data and the elemental contents for all samples are reported in Table 1, and the SEM images (Backscattered-Electron and X-Ray mapping) for the nine chondrules are showed in Figures A1 and A2 in the Appendix. The measured $\epsilon^{53}\text{Cr}$ and $\epsilon^{54}\text{Cr}$ values for bulk Sahara 97096 of 0.19 ± 0.04 and -0.01 ± 0.14 (2SE, $N = 11$), respectively, are indistinguishable from previously reported values for other ECs (Trinquier et al. 2007, 2008b; Qin et al. 2010; Mougél et al. 2018). The Allende data (both Mn/Cr ratio and isotope composition; Table 1) are also consistent with those reported in previous studies (Shukolyukov & Lugmair 2006; Trinquier et al. 2007, 2008b; Qin et al. 2010). Combined with our consistent data for terrestrial samples in Zhu et al. (2019b), these results confirm the accuracy of our approach.

The $\epsilon^{54}\text{Cr}$ data for all the chondrules average at 0.11, but they can be divided into two distinct groups. Group A has indistinguishable $\epsilon^{54}\text{Cr}$ values with an average of -0.11 ± 0.13 (2SD, $N = 7$), which is slightly lower to that of bulk Sahara 97096 ($\epsilon^{54}\text{Cr} = -0.01 \pm 0.14$). In contrast, two anomalous chondrules (Group B), KF8 and KF9, show positive $\epsilon^{54}\text{Cr}$ values

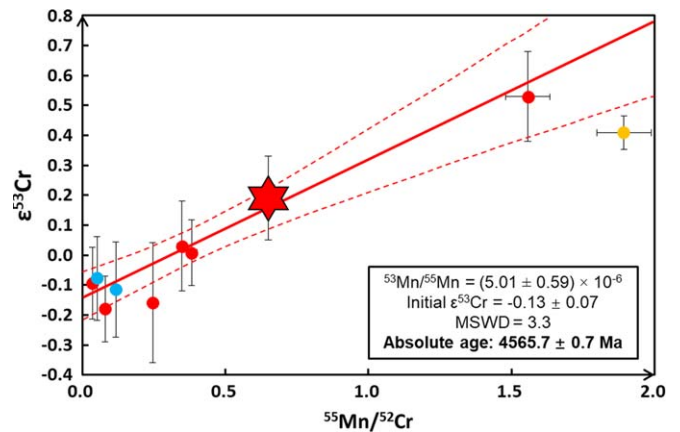


Figure 1. ^{53}Mn – ^{53}Cr isochron for bulk chondrules from enstatite chondrites. The red, orange, and blue circles are EC chondrules for typical A (EC-like), high Fe-content Group A (KF4), and Group B (anomalous; KF8 and KF9), respectively. The red hexagram represents the bulk Sahara 97096 chondrite composition. The uncertainty (2σ) for $^{55}\text{Mn}/^{52}\text{Cr}$ is 5%. However, this isochron does not include the bulk Sahara 97096 chondrite, and does not include the two anomalous chondrules in Group B (blue circles) and the Fe-rich chondrule (orange). The uncertainty for the slope (dashed lines) is reported with 2σ .

of 1.01 ± 0.11 and 0.32 ± 0.11 , despite having a similar chemical composition to Group A chondrules. The anomalous $\epsilon^{54}\text{Cr}$ cannot be explained by the influence of equilibrium mass-dependent fractionation, given that the $\epsilon^{53}\text{Cr}$ values do not co-vary with the $\epsilon^{54}\text{Cr}$ signatures. KF4 chondrule is characterized by the high content of sulfide minerals (Figures A1 and A2) and Fe. With the exception of KF4, the $\epsilon^{53}\text{Cr}$ values of the six Group A chondrules and the bulk Sahara 97096 chondrite correlate with their $^{55}\text{Mn}/^{52}\text{Cr}$ ratios. A model 1 regression of these data using *IsoplotR* (Vermeesch 2018) yields a slope of 0.442 ± 0.052 (2σ) that corresponds to a $^{53}\text{Mn}/^{55}\text{Mn}$ ratio of $(5.01 \pm 0.59) \times 10^{-6}$ (2σ) and an initial $\epsilon^{53}\text{Cr}$ of -0.13 ± 0.07 (MSWD = 3.3; Figure 1). If the bulk Sahara 97096 is not included in the isochron, the slope (0.420 ± 0.054 , 2σ) and initial $\epsilon^{53}\text{Cr}$ (-0.13 ± 0.07 ; MSWD = 3.2) is the same as the previous values within uncertainty. There is also no correlation between $\epsilon^{53}\text{Cr}$ and $\epsilon^{54}\text{Cr}$ for all the chondrules (Figure 2).

It should be noted that this Mn–Cr correlation line for the EC chondrules is highly controlled by one high-Mn/Cr chondrule,

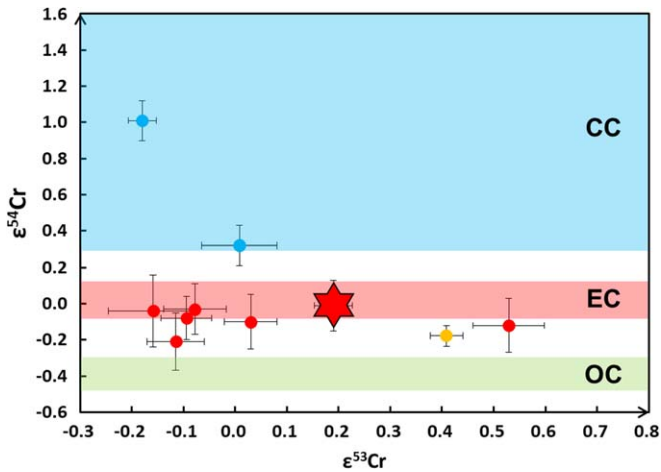


Figure 2. The blue, red, and green bars represent the $\epsilon^{54}\text{Cr}$ for carbonaceous, enstatite, and ordinary chondrites, respectively, with literature data (Trinquier et al. 2007; Qin et al. 2010; Mougél et al. 2018; Pedersen et al. 2019; Zhu et al. 2020a). The red and orange (KF4; Fe-rich) circles are Group A chondrites, while the blue ones are the two Group B chondrites (KF8 and KF9), with the bulk Sahara 97096 of red hexagram.

KF2. The high Mn/Cr ratio for KF2 can be caused by some Mn-rich sulfides that formed simultaneously with the chondrites (Piani et al. 2016). If we do not consider it, the remaining chondrites and bulk Sahara 97096 would form a slightly older isochron with slope of 0.485 ± 0.090 and initial $\epsilon^{53}\text{Cr}$ of -0.14 ± 0.09 (2σ , MSWD = 3.7), which corresponding to an $^{53}\text{Mn}/^{55}\text{Mn}$ of $(5.50 \pm 1.02) \times 10^{-6}$.

4. Discussion

4.1. Outer Solar System Materials Contamination

The bulk silicate Earth ($\epsilon^{54}\text{Cr} = 0.09 \pm 0.12$; 2SD, $N = 17$, (Trinquier et al. 2007; Mougél et al. 2018; Zhu et al. 2020a), the Moon ($\epsilon^{54}\text{Cr} = 0.09 \pm 0.08$; Mougél et al. 2018), and aubrite meteorites ($\epsilon^{54}\text{Cr} = 0.03 \pm 0.18$; 2SD, $N = 8$ including Shallowater; Zhu et al. 2020b) have similar $\epsilon^{54}\text{Cr}$ values compared to ECs ($\epsilon^{54}\text{Cr} = 0.02 \pm 0.10$; 2SD, $N = 12$; Trinquier et al. 2007; Qin et al. 2010; Mougél et al. 2018), whereas most other solar system materials have variable and distinct compositions (Trinquier et al. 2007). The similar isotopic composition for Cr (and many other elements) forms the basis for models suggesting the Earth’s building blocks were EC-like (Javoy et al. 2010). Based on the chondrule accretion model (Johansen et al. 2015), chondrules may represent the building blocks for planetary embryos. Therefore, EC chondrules, which are hosted in chondrites that have similar isotope compositions to that of the Earth, may be possible candidates for the precursors from which the Earth–Moon system accreted, although the ECs’ bulk chemical composition (e.g., Mg/Si ratio) does not match that of Earth (e.g., Alexander 2019). The average $\epsilon^{54}\text{Cr}$ value of all the nine chondrules analyzed here, ~ 0.06 , is indistinguishable from that of the bulk sample ($\epsilon^{54}\text{Cr} = -0.01 \pm 0.14$) and the Earth ($\epsilon^{54}\text{Cr} = 0.09 \pm 0.12$), indicating a similar isotopic composition of the precursor material of the Earth and EC chondrules.

In details (Figure 2), the $\epsilon^{54}\text{Cr}$ of seven Group A chondrites have with $\epsilon^{54}\text{Cr} = -0.11 \pm 0.13$ (2SD, $N = 7$), which is slightly lower than for bulk EC and the Earth. The two Group B have distinctively higher $\epsilon^{54}\text{Cr}$ values falling within the range of $\epsilon^{54}\text{Cr}$ compositions defined by carbonaceous chondrites that

vary from 0.3 to 1.6 (Trinquier et al. 2007; Qin et al. 2010; Zhu et al. 2020a). As such, when taken individually none of the two groups of chondrules have $\epsilon^{54}\text{Cr}$ signatures that match the Earth, although the seven Group A chondrules may represent the primitive EC precursors. Contamination of these EC with outer solar system material characterized by carbonaceous chondrite $\epsilon^{54}\text{Cr}$ signatures may explain the raised $\epsilon^{54}\text{Cr}$ compositions of both bulk EC and bulk silicate Earth. However, the two anomalous Group B chondrules do not show any distinct petrological or chemical features (see Figures A1 and A2, Mg# and Fe/Cr). This indicates that the addition of CC material predates the formation of these EC chondrules, because the two chondrules are also dominated by enstatites and only show the EC-like petrology and chemistry, which means that CC-like features have been erased by the formation process of EC chondrules. The chemical composition for the Group B chondrules is similar to that of Group A chondrules, indicating that the carbonaceous chondrite material was also chemically similar to EC chondrules (e.g., low Fe content). However, Group B chondrules have elevated $\epsilon^{54}\text{Cr}$ signatures compared to Group A chondrules. A possibility is that the Group B enstatite chondrule precursors were contaminated with CI chondrite-like material, which are characterized by the highest $\epsilon^{54}\text{Cr}$ values (1.53 ± 0.07 ; 2SD, defined by $\epsilon^{54}\text{Cr}$ of Orgueil and Ivuna; Schiller et al. 2014; Zhu et al. 2020a). This is unlikely because CI chondrites also possess much higher Fe/Cr (~ 68) and lower Mg# (~ 53) compared to the EC chondrules in this study (Barrat et al. 2012). A similar issue exists when considering contamination with matrix material from all other carbonaceous chondrites, given that this material is typically characterized by high Fe content (Hezel & Palme 2010; Palme et al. 2015). A possible mechanism to explain Group B chondrules is admixing of carbonaceous chondrite chondrules in the accretion region of the EC chondrite parent body as carbonaceous chondrite chondrules are characterized by high $\epsilon^{54}\text{Cr}$ (Yamashita et al. 2010; Olsen et al. 2016; Zhu et al. 2019a) but have similar Mg# and Fe/Cr ratios compared to EC chondrules (Hezel & Palme 2010; Palme et al. 2015). The two Group B chondrules also defined a regression with slope of 0.63 ± 0.13 (corresponding to an $^{53}\text{Mn}/^{55}\text{Mn}$ ratio of $(7.1 \pm 1.5) \times 10^{-6}$; an initial $\epsilon^{53}\text{Cr}$ of -0.23 ± 0.02 ; MSWD = 1) that is the same as the Mn–Cr isochron defined by chondrules in CO carbonaceous chondrite (Zhu et al. 2019a); however, they also fall on the isochron defined by the Group A chondrules within uncertainty. As such, this may indicate a mixing origin of Group B chondrules between EC chondrule and carbonaceous chondrite chondrule precursor material. This $\epsilon^{54}\text{Cr}$ variation cannot be caused the $\epsilon^{54}\text{Cr}$ heterogeneity in the EC accretion region, because the seven Group A chondrules demonstrate homogeneous $\epsilon^{54}\text{Cr}$ values, and only two chondrules (Group B) show positive $\epsilon^{54}\text{Cr}$ values. This observation is also supported by the fact that a few olivine grains in EC chondrules are characterized by CC-like O isotope features (Weisberg et al. 2011). Furthermore, the reduced ECs most likely formed in the inner solar system, whereas the oxidized carbonaceous chondrites accreted in the outer solar system (Morbidelli et al. 2012). As such, the observation that CC-like material contributed to EC chondrules is consistent with inward transportation of outer solar system solids to the inner solar system as suggested by dynamical modeling (Weidenschilling 1980), but does not support the chondrule–matrix complementarity within ECs, which needs all chondrule materials and also matrix to come

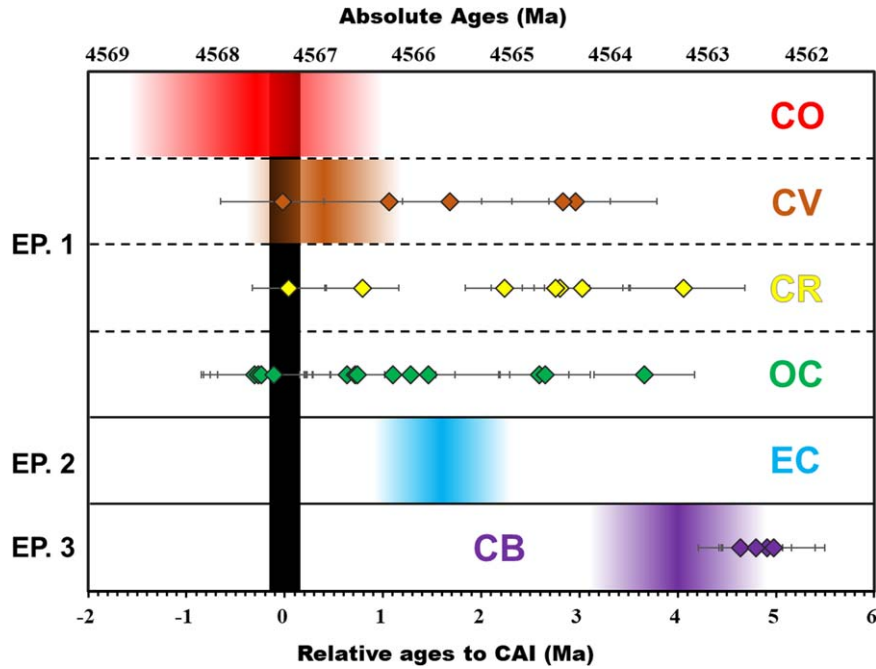


Figure 3. Review of Mn–Cr ages (external isochron, chondrule precursor ages, instead of the average last-melting ages) and U-corrected Pb–Pb ages (internal isochron, last-melting ages) of chondrules from different groups of chondrites. The diamonds are Pb–Pb ages, while the bars are Mn–Cr ages (except for the black bar, which indicates the age of CAIs). The chondrule precursor age should be older than or similar to all their last-melting ages. The Mn–Cr age data are from this study and literature data (Yin et al. 2009; Yamashita et al. 2010; Zhu et al. 2019a), and the U-corrected Pb–Pb age data are from these literature (Connelly et al. 2012; Bollard et al. 2015, 2017). Note that, it is debatable whether ^{26}Al is homogeneously distributed in the solar system (Larsen et al. 2011; Bollard et al. 2019; Gregory et al. 2020), so we decided not to include the Al–Mg ages for chondrules in this figure, both for the in situ dating (Nagashima et al. 2018) and bulk isochron ages (e.g., Luu et al. 2015). It can be seen that there are three epochs for chondrule formation: Epoch (EP) 1 is the formation of typical silicate chondrules (e.g., silicate CC and OC chondrules); EP 2 is the formation of EC chondrules via silicate-gas reaction; EP 3 is the formation of metal-rich (e.g., CB) chondrules via impact.

from the same reservoir (Hezel et al. 2018). The contribution of carbonaceous material to the terrestrial planet accretion regions within the first 2 Ma of our solar system’s formation is consistent with the idea of an early and rapid secular evolution of the solids accreting to the growing proto-Earth, as inferred from the Ca and Fe isotopic signatures of inner solar system objects (Schiller et al. 2018, 2020).

4.2. Protracted Formation of EC Chondrite Chondrules

The KF4 chondrule has the highest Fe/Cr ratio (18.1) and lowest Mg# (88) among the Group A chondrules. The elemental mapping also reveals that this chondrule contains significantly more sulfide (with higher Fe than the enstatites) than the other chondrules. According to the chemical features of the sulfides in KF4 (rich in Fe, Cr, Mn, and Ti and poor in Ca), we speculated that they are niningerite that formed simultaneously with the chondrules (Piani et al. 2016). However, the in situ Mn–Cr dating for the sulfides outside the chondrules in ECs show their $^{53}\text{Mn}/^{55}\text{Mn}$ ratios are less than 1×10^{-6} (Wadhwa et al. 1997; Guan et al. 2007), indicating the sulfides are usually young. Therefore, it is possible that the mild metamorphism effect caused diffusion of Fe, Cr, and other elements from sulfides to the chondrule, making KF4 below the isochron formed by other normal Group A chondrules (Figure 1). This is consistent with the KF4 petrology that it is surrounded by some sulfides (Figure A2, left and right).

The correlation line between $^{55}\text{Mn}/^{52}\text{Cr}$ ratios and $\epsilon^{53}\text{Cr}$ values for bulk Sahara 97096 and other six Group A chondrules can be interpreted as a Mn–Cr isochron, which reflects the decay of live ^{53}Mn in the early solar system. The slope of the isochron returns a $^{53}\text{Mn}/^{55}\text{Mn}$ ratio of $(3.37 \pm 0.27) \times 10^{-6}$ that, when anchored to

the D’Orbigny angrite, which has a U-corrected ^{207}Pb – ^{206}Pb age of 4563.37 ± 0.25 Ma (Amelin 2008; Brennecka & Wadhwa 2012) and a fossilized $^{53}\text{Mn}/^{55}\text{Mn}$ abundance of $(3.24 \pm 0.04) \times 10^{-6}$ (Glavin et al. 2004; Amelin 2008), corresponds to an absolute age of 4565.7 ± 0.7 Ma (2σ). The age uncertainty reflects propagated uncertainties on the slope of the isochron, the half-life of ^{53}Mn , the U-corrected Pb–Pb age, and the $^{53}\text{Mn}/^{55}\text{Mn}$ ratio of D’Orbigny. This age is best understood to reflect that Mn/Cr fractionation recorded by the EC chondrules occurred 1.6 ± 0.7 Ma after formation of the solar system (dated by CAIs, the first solar system solids; Amelin et al. 2010; Connelly et al. 2012). It should be noted that the isochron would stay the same if the bulk Sahara 97096 was considered, suggesting the six Group A chondrules come from the Sahara 97096 reservoir. Compared to their host meteorite Sahara 97096 that has a bulk $^{55}\text{Mn}/^{52}\text{Cr}$ ratio of 0.65, the chondrules are characterized by both lower and higher $^{55}\text{Mn}/^{52}\text{Cr}$ ratios ranging from 0.04 to 1.89. These variable Mn/Cr ratios may be the product of variable evaporation and re-condensation histories experienced by the individual chondrules during their formation given the volatility difference between Mn and Cr (Lodders 2003; Sossi et al. 2019) or due to a secular evolution of the silicate-gas environment during chondrule formation itself resulting in the sequential formation of phases with variable Mn/Cr ratios that were incorporated variably into individual chondrules (Piani et al. 2016; Tanaka & Nakamura 2017). Either way, because the chondrules falls onto a single isochron, the processes at the origin of the Mn/Cr fractionation occurred within the uncertainty on the slope, which corresponds to 1.4 Ma.

We emphasize that the age of the event deduced from this bulk isochron (as opposed to internal isochrons) corresponds to the formation of chondrule precursors, rather than the average

ages of chondrule last-melting events. Therefore, this age must predate or being similar to ages determined from internal isochron of individual chondrules (e.g., Zhu et al. 2019b), and can be compared to the oldest chondrules in a given chondrite group. The formation of the EC chondrule precursors, as dated here, took place after that of most carbonaceous chondrite (Yin et al. 2009; Connelly et al. 2012; Bollard et al. 2017; Zhu et al. 2019a) and ordinary chondrite chondrules (Yin et al. 2007; Connelly et al. 2012; Bollard et al. 2017). On the other hand, EC chondrules predate metal-rich chondrules found in CB and CH chondrites, which formed 4.8 ± 0.3 Ma after CAIs (4567.30 ± 0.16 Ma; Connelly et al. 2012; Krot et al. 2005; Yamashita et al. 2010; Bollard et al. 2015). As such, our results indicate the presence of at least three major periods for chondrule formation in the early solar system (Figure 3): first, early formation of carbonaceous chondrite and ordinary chondrite chondrules that began concurrently with CAIs formation at the beginning of the solar system. This was followed by EC chondrule formation by gas-melt interactions (Lehner et al. 2013; Tanaka & Nakamura 2017) ~ 1.6 Ma later. Lastly, another three million years later (~ 4.8 Ma), the metal-rich CB and CH chondrules were produced by planetary impacts (Krot et al. 2005; Yamashita et al. 2010; Bollard et al. 2015).

Finally, because this isochron is highly controlled by the KF2 chondrule, which has the highest Mn/Cr ratio. If this chondrule is not considered, the rest of chondrules and bulk Sahara 97096 would form a slightly older isochron with slope of 0.485 ± 0.090 and initial $\epsilon^{53}\text{Cr}$ of -0.14 ± 0.09 (2σ , $\text{MSWD} = 3.7$), which, corresponding to an $^{53}\text{Mn}/^{55}\text{Mn}$ of $(5.50 \pm 1.02) \times 10^{-6}$ and the absolute age of 4566.2 ± 1.1 Ma (i.e., 1.1 ± 1.1 Ma after CAIs) anchored to U-corrected D'Orbigny. Although this age is the same as the that of previous isochron (4565.7 ± 0.7 Ma, with KF2) within uncertainty, it is possible that the formation of EC chondrules is older.

5. Conclusion

Chondrules in the primitive EH3 chondrite (Sahara 97096) were extracted by microdrill method, and their mass-independent Cr isotope compositions were measured by the TIMS with

total-evaporation method. The achievements about the origin of EC chondrules are as follows.

1. Based on the $^{54}\text{Cr}/^{52}\text{Cr}$ ratios, all the chondrules can be divided into two groups: the EC-like ($\epsilon^{54}\text{Cr} = -0.11 \pm 0.13$; 2SD , $N = 7$) and the CC-like with the $\epsilon^{54}\text{Cr}$ value of ~ 1.01 and ~ 0.32 . This suggests the materials in the outer solar system (CC accretion region) were transported to EC accretion region (inner solar system), and contaminated some EC chondrules.
2. The EC-like chondrules (except a high-Fe one) and bulk Sahara 97096 chondrite form a well-defined Mn–Cr isochron, corresponding to an absolute age of 4565.7 ± 0.7 Ma, i.e., 1.6 ± 0.7 Ma after CAIs. The formation of EC chondrules postdated the typical silicate chondrules in CV, CO, CR, and OC chondrites, but predated the metal-rich CB chondrules, suggesting three epochs for chondrule formation process in the early solar system.

We thank the efficient editorial handling from AAS scientific editor, Prof. Maria Womack and constructive comments from an anonymous reviewer, especially during the COVID-19 period. F.M. acknowledges funding from the European Research Council under the H2020 framework program/ERC grant agreement (#637503-Pristine) and financial support of the UnivEarthS Labex program at University of Paris. M.B. acknowledges funding from the Danish National Research Foundation (#DNRF97) and the European Research Council (#616027-Stardust2Asteroids). Parts of this work were supported by IGP multidisciplinary program PARI, and by Paris–IdF region SESAME (#12015908). Stephan Borensztajn, Elisheva van Kooten, Daniel Wielandt, and Pierre Burckel are appreciated for assistance in SEM, Microdrill, TIMS, and ICP-MS work, respectively. K.Z. thanks the China Scholarship Council for a PhD fellowship (#201706340161).

Appendix

In this appendix, we mainly show the SEM images of the nine enstatite chondrules. Figure A1 is the Backscattered-Electron images, while the X-ray elemental mapping images are demonstrated in Figure A2.

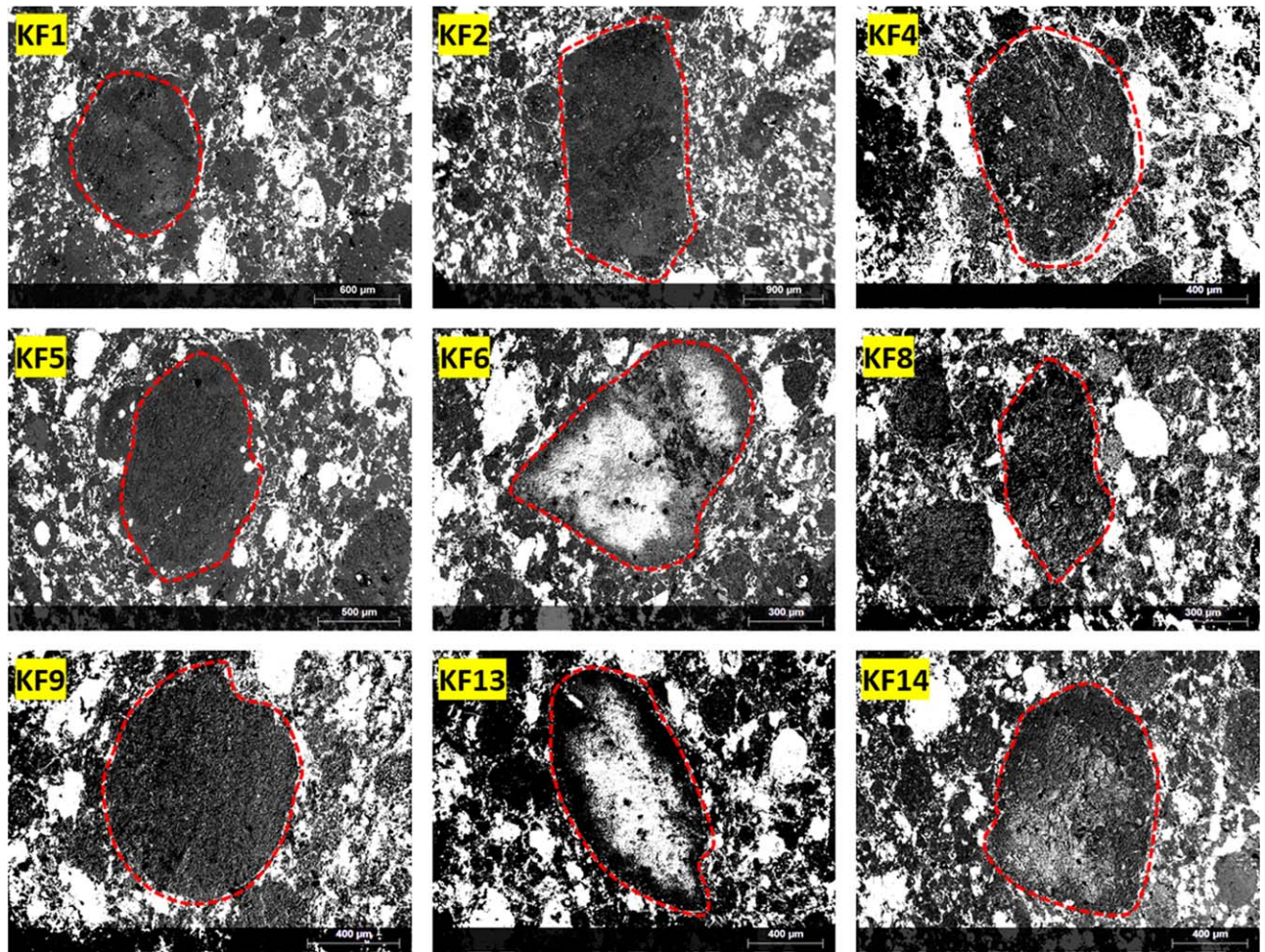


Figure A1. Backscattered-Electron images for the selected chondrules. The red dashed lines point to the chondrules.

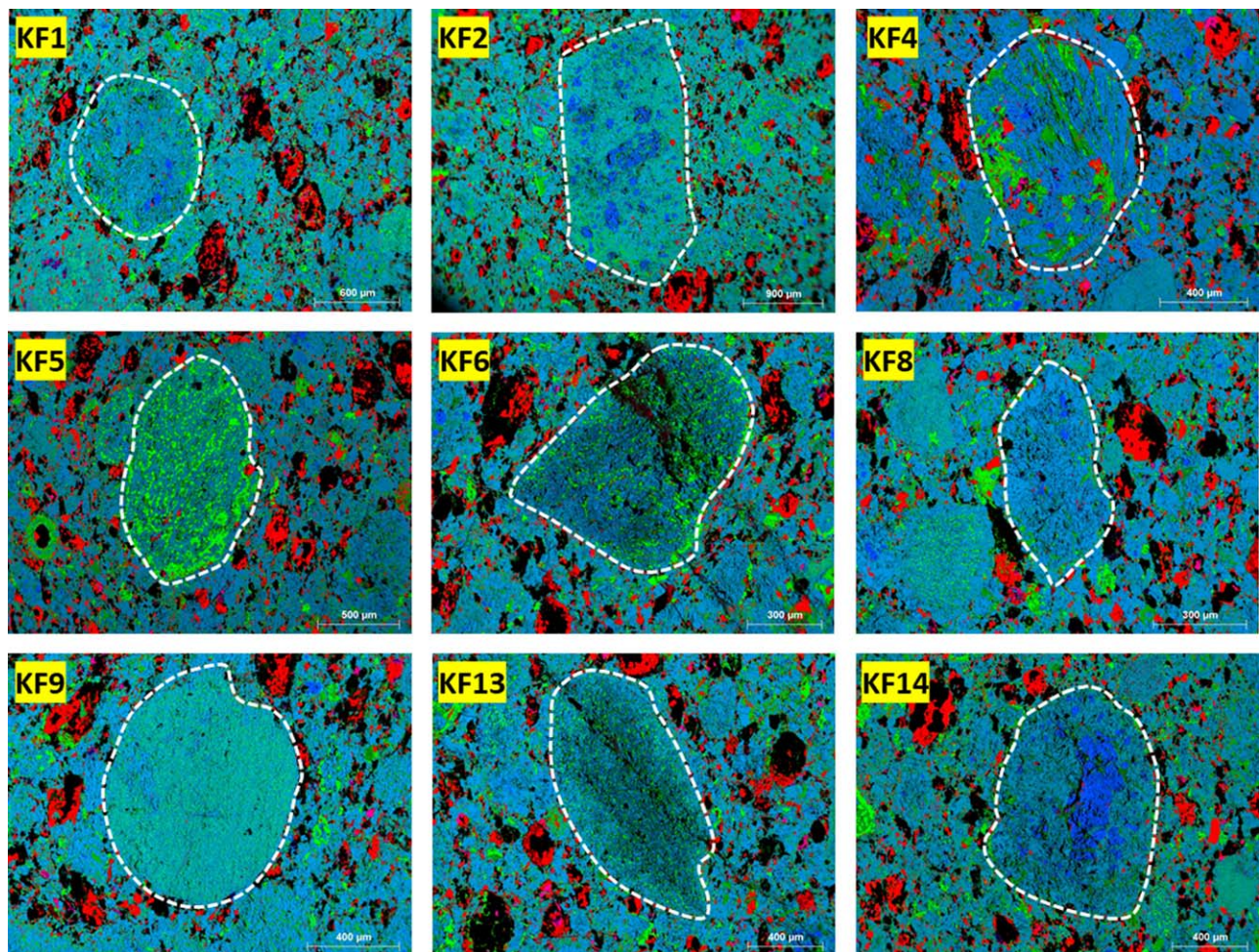


Figure A2. Combined S–Mg–Si (red–blue–green) X-ray elemental images of selected chondrules from Sahara 97096 chondrite investigated in this study. Note that the red spots in KF4 (High-Fe) are sulfides that are rich in Fe, Cr, Mn, and Ti and poor in Ca (mostly niningerite). These sulfide minerals inside chondrules are magmatic, formed at the same time during chondrule formation (Piani et al. 2016). However, around the KF4 chondrule rim, there are some sulfides of which the $^{53}\text{Mn}/^{55}\text{Mn}$ ratios are less than 1×10^{-6} (Wadhwa et al. 1997; Guan et al. 2007). It is possible that the mild metamorphism effect caused the diffusion of sulfides into the chondrule, making the chondrule have high Fe content and young Cr, and furthermore locating KF4 below the bulk Mn–Cr isochron for EC chondrules.

ORCID iDs

Ke Zhu (朱柯) <https://orcid.org/0000-0003-3613-7239>
 Martin Schiller <https://orcid.org/0000-0003-4149-0627>
 Martin Bizzarro <https://orcid.org/0000-0001-9966-2124>

References

- Alexander, C. M. O. D. 2019, *GeCoA*, 254, 246
 Alexander, C. O. D., Grossman, J., Ebel, D., & Ciesla, F. 2008, *Sci*, 320, 1617
 Amelin, Y. 2008, *GeCoA*, 72, 221
 Amelin, Y., Kaltenbach, A., Iizuka, T., et al. 2010, *E&PSL*, 300, 343
 Amelin, Y., Koefoed, P., Iizuka, T., et al. 2019, *GeCoA*, 245, 628
 Barrat, J. A., Zanda, B., Moynier, F., et al. 2012, *GeCoA*, 83, 79
 Birck, J.-L., & Allègre, C. J. 1988, *Natur*, 331, 579
 Bizzarro, M., Paton, C., Larsen, K., et al. 2011, *J. Anal. At. Spectrom.*, 26, 565
 Bollard, J., Connelly, J. N., & Bizzarro, M. 2015, *M&PS*, 50, 1197
 Bollard, J., Connelly, J. N., Whitehouse, M. J., et al. 2017, *SciA*, 3, e1700407
 Bollard, J., Kawasaki, N., Sakamoto, N., et al. 2019, *GeCoA*, 260, 62
 Brennecke, G. A., & Wadhwa, M. 2012, *PNAS*, 109, 9299
 Budde, G., Burkhardt, C., Brennecke, G. A., et al. 2016a, *E&PSL*, 454, 293
 Budde, G., Kleine, T., Kruijjer, T. S., Burkhardt, C., & Metzler, K. 2016b, *PNAS*, 113, 2886
 Budde, G., Kruijjer, T. S., & Kleine, T. 2018, *GeCoA*, 222, 284
 Connelly, J. N., & Bizzarro, M. 2016, *E&PSL*, 452, 36
 Connelly, J. N., & Bizzarro, M. 2018, in *Chondrules: Records of Protoplanetary Disk Processes*, ed. A. N. Krot, H. C. Connolly, Jr., & S. S. Russell (Cambridge: Cambridge Univ. Press), 300
 Connelly, J. N., Bizzarro, M., Krot, A. N., et al. 2012, *Sci*, 338, 651
 Coplen, T. B., Böhlke, J. N., De Bièvre, P., et al. 2002, *P&PCh*, 74, 1987
 Ebel, D. S., & Alexander, C. M. O. D. 2011, *P&SS*, 59, 1888
 Glavin, D., Kubny, A., Jagoutz, E., & Lugmair, G. 2004, *M&PS*, 39, 693
 Göpel, C., Birck, J.-L., Galy, A., Barrat, J.-A., & Zanda, B. 2015, *GeCoA*, 156, 1
 Gregory, T., Luu, T.-H., Coath, C. D., Russell, S. S., & Elliott, T. 2020, *SciA*, 6, eaay9626
 Guan, Y., Huss, G. R., & Leshin, L. A. 2007, *GeCoA*, 71, 4082
 Guan, Y., Huss, G. R., Leshin, L. A., MacPherson, G. J., & McKeegan, K. D. 2006, *M&PS*, 41, 33
 Hewins, R. H. 1997, *AREPS*, 25, 61
 Hezel, D. C., Bland, P. A., Palme, H., Jacquet, E., & Bigolski, J. 2018, in *Chondrules: Records of Protoplanetary Disk Processes*, ed. A. N. Krot, H. C. Connolly, Jr., & S. S. Russell (Cambridge: Cambridge Univ. Press), 91
 Hezel, D. C., & Palme, H. 2010, *E&PSL*, 294, 85
 Inglis, E. C., Creech, J. B., Deng, Z., & Moynier, F. 2018, *ChGeo*, 493, 544
 Jacquet, E., Piani, L., & Weisberg, M. K. 2018, in *Chondrules: Records of Protoplanetary Disk Processes*, ed. A. N. Krot, H. C. Connolly, Jr., & S. S. Russell (Cambridge: Cambridge Univ. Press), 175
 Javoy, M., Kaminski, E., Guyot, F., et al. 2010, *E&PSL*, 293, 259
 Johansen, A., Low, M.-M. M., Lacerda, P., & Bizzarro, M. 2015, *SciA*, 1, e1500109
 Krot, A. N., Amelin, Y., Cassen, P., & Meibom, A. 2005, *Natur*, 436, 989
 Larsen, K. K., Trinquier, A., Patron, C., et al. 2011, *ApJL*, 735, L37
 Larsen, K. K., Wielandt, D., & Bizzarro, M. 2018, *J. Anal. At. Spectrom.*, 33, 613
 Larsen, K. K., Wielandt, D., Schiller, M., & Bizzarro, M. 2016, *J. Chromatogr. A*, 1443, 162

- Lehner, S. W., Petaev, M. I., Zolotov, M. Y., & Buseck, P. R. 2013, *GeCoA*, **101**, 34
- Lodders, K. 2003, *ApJ*, **591**, 1220
- Lugmair, G., & Shukolyukov, A. 1998, *GeCoA*, **62**, 2863
- Luu, T.-H., Young, E. D., Gounelle, M., & Chaussidon, M. 2015, *PNAS*, **112**, 1298
- Morbidelli, A., Lunine, J., O'Brien, D., Raymond, S., & Walsh, K. 2012, *AREPS*, **40**, 251
- Mougel, B., Moynier, F., & Göpel, C. 2018, *E&PSL*, **481**, 1
- Moynier, F., & Fegley, B., Jr 2015, in *The Early Earth: Accretion and Differentiation*, Geophysical Monograph Series, Vol. 212, ed. J. Badro & M. Walter (Hoboken, NJ: Wiley), 27
- Nagashima, K., Kita, N. T., & Luu, T.-H. 2018, in *Chondrules: Records of Protoplanetary Disk Processes*, ed. A. N. Krot, H. C. Connolly, Jr., & S. S. Russell (Cambridge: Cambridge Univ. Press), 247
- Nittler, L. R., & Weider, S. Z. 2019, *Elements: Int. Mag. Mineral. Geochem. Petrol.*, 15, 33
- Olsen, M. B., Wielandt, D., Schiller, M., van Kooten, E. M. M. E., & Bizzarro, M. 2016, *GeCoA*, **191**, 118
- Palme, H., Hezel, D. C., & Ebel, D. S. 2015, *E&PSL*, **411**, 11
- Patzer, A., & Schultz, L. 2001, *M&PS*, **36**, 947
- Pedersen, S. G., Schiller, M., Connelly, J. N., & Bizzarro, M. 2019, *M&PS*, **54**, 1215
- Piani, L., Marrocchi, Y., Libourel, G., & Tissandier, L. 2016, *GeCoA*, **195**, 84
- Qin, L., Alexander, C. M. O. D., Carlson, R. W., Horan, M. F., & Yokoyama, T. 2010, *GeCoA*, **74**, 1122
- Qin, L., Nittler, L. R., Alexander, C. M., et al. 2011, *GeCoA*, **75**, 629
- Quirico, E., Bourrot-denise, M., Robin, C., Montagnac, G., & Beck, P. 2011, *GeCoA*, **75**, 3088
- Sanborn, M. E., Wimpenny, J., Williams, C. D., et al. 2019, *GeCoA*, **245**, 577
- Schiller, M., Bizzarro, M., & Fernandes, V. A. 2018, *Natur*, **555**, 507
- Schiller, M., Bizzarro, M., & Siebert, J. 2020, *SciA*, **6**, eaay7604
- Schiller, M., van Kooten, E., Holst, J. C., Olsen, M. B., & Bizzarro, M. 2014, *J. Anal. At. Spectrom.*, **29**, 1406
- Schneider, D., Symes, S., Benoit, P., & Sears, D. 2002, *M&PS*, **37**, 1401
- Shukolyukov, A., & Lugmair, G. 2006, *E&PSL*, **250**, 200
- Sossi, P. A., Klemme, S., O'Neill, H. S. C., Berndt, J., & Moynier, F. 2019, *GeCoA*, **260**, 204
- Tanaka, R., & Nakamura, E. 2017, *NatAs*, **1**, 0137
- Trinquier, A., Birck, J.-L., & Allègre, C. J. 2007, *ApJ*, **655**, 1179
- Trinquier, A., Birck, J.-L., & Allègre, C. J. 2008a, *J. Anal. At. Spectrom.*, **23**, 1565
- Trinquier, A., Birck, J. L., Allègre, C. J., Göpel, C., & Ulfbeck, D. 2008b, *GeCoA*, **72**, 5146
- van Kooten, E. M. M. E., Schiller, M., & Bizzarro, M. 2017, *GeCoA*, **208**, 1
- van Kooten, E. M. M. E., Wielandt, D., Schiller, M., et al. 2016, *PNAS*, **113**, 2011
- Vermeesch, P. 2018, *Geosci. Front.*, **9**, 1479
- Wadhwa, M., Zinner, E. K., & Crozaz, G. 1997, *M&PS*, **32**, 281
- Wasson, J. T. 1988, in *Mercury*, ed. F. Vilas, C. R. Chapman, & M. S. Matthews (Tucson, AZ: Univ. Arizona Press), 622
- Weidenschilling, S. 1980, *Icar*, **44**, 172
- Weisberg, M. K., Ebel, D. S., Connolly, H. C., Jr, Kita, N. T., & Ushikubo, T. 2011, *GeCoA*, **75**, 6556
- Weisberg, M. K., & Kimura, M. 2012, *ChEG*, **72**, 101
- Yamashita, K., Maruyama, S., Yamakawa, A., & Nakamura, E. 2010, *ApJ*, **723**, 20
- Yin, Q., Jacobsen, B., Moynier, F., & Hutcheon, I. D. 2007, *ApJL*, **662**, L43
- Yin, Q., Yamashita, K., Yamakawa, A., et al. 2009, *LPSC*, **40**, 2006
- Zhang, J., Dauphas, N., Davis, A. M., Leya, I., & Fedkin, A. 2012, *NatGe*, **5**, 251
- Zhu, K., Liu, J., Moynier, F., et al. 2019a, *ApJ*, **873**, 82
- Zhu, K., Moynier, F., Barrat, J.-A., et al. 2019b, *ApJL*, **877**, L13
- Zhu, K., Moynier, F., Schiller, M., et al. 2020a, *SciA*, submitted
- Zhu, K., Moynier, F., Schiller, M., et al. 2020c, *ApJ*, **888**, 126
- Zhu, K., Moynier, F., Schiller, M., & Bizzarro, M. 2020b, *E&PSL*, submitted